TSUNAMI BENCHMARK RESULTS FOR FULLY NONLINEAR BOUSSINESQ WAVE MODEL FUNWAVE-TVD, VERSION 1.0

BY

BABAK TEHRANIRAD, FENGYAN SHI AND JAMES T. KIRBY

CENTER FOR APPLIED COASTAL RESEARCH, UNIVERSITY OF DELAWARE,

NEWARK, DE

JEFFREY C. HARRIS AND STEPHAN GRILLI

DEPARTMENT OF OCEAN ENGINEERING, UNIVERSITY OF RHODE ISLAND,

NARRAGANSETT, RI

RESEARCH REPORT NO. CACR-11-02
JUNE 2011

This study was supported by the National Tsunami Hazard Mitigation Program

CENTER FOR APPLIED COASTAL RESEARCH

Ocean Engineering Laboratory
University of Delaware
Newark, Delaware 19716

Abstract

This report describes tsunami benchmark testing of the Boussinesq model FUNWAVE-TVD, carried out in conjunction with the National Tsunami Hazard Mitigation Program, MMS Tsunami Inundation Model Validation Workshop, March 28 - April 1, 2011. The results presented here represent testing of Version 1.0 of the code, and will be updated online at http://chinacat.coastal.udel.edu/~kirby/progrsams/funwave/funwave.html with each version change for the publicly distributed code.

This work was supported by the National Tsunami Hazard Mitigation Program.

Contents

List of Figures

List of Tables

1 Introduction

This report describes the benchmark testing of the Boussinesq model FUNWAVE-TVD which has been carried out as part of the Benchmark Workshop exercise for the National Tsunami Hazard Mitigation Program. The benchmark tests described here are taken from Synolakis et al (2007). The report is organized as follows. Section 2 provides a description of the model equations and numerical scheme. Section 3 provides basic information on hydrodynamic considerations used to judge basic model validity. Sections 4 and 5 describe benchmark tests for analytical and laboratory cases, respectively.

Data for each benchmark are obtained from http://nctr.pmel.noaa.gov/benchmark/

FUNWAVE-TVD is distributed as open source code. General users may obtain the most recent tested version from the web site

http://chinacat.coastal.udel.edu/k̃irby/programs/funwave/funwave.html

which provides this code along with other programs developed at the Center for Applied Coastal Research. The code is provided along with a unix/linux makefile, a users manual (Shi et al, 2011b), and input files for executing the tests described in the manual. The present report will also be updated with each major change in program version. Input files and scripts for executing the benchmark tests described here are provided at the website given above

Version control for FUNWAVE-TVD is done using Mercurial (O'Sullivan, 2009). Users who would like to become part of the development team should contact Fengyan Shi (fyshi@udel.edu) or Jim Kirby (kirby@udel.edu).

2 Model description

In this section, we describe the set of Boussinesq equations which are used as the basis for FUNWAVE-TVD. FUNWAVE-TVD is formulated in both Cartesian coordinates and in spherical (lat-long) coordinates for application to ocean basin scale problems. The benchmarks considered here are all treated in Cartesian coordinates, and we therefore omit description of the spherical coordinate model. This may be found in Shi et al (2011b). We retain dimensional forms below but will refer to the apparent $O(\mu^2)$ ordering of terms resulting from deviations from hydrostatic behavior in order to identify these effects as needed. Here. μ is a parameter characterizing the ratio of water depth to wave length, and is assumed to be small in classical Boussinesq theory. The model equations used here follow from the work of Chen (2006). In this and earlier works starting with Nwogu (1993), the horizontal velocity is written as

$$\mathbf{u} = \mathbf{u}_\alpha + \mathbf{u}_2(z) \tag{1}$$

Here, $\mathbf{u}_\alpha$ denotes the velocity at a reference elevation $z = z_\alpha$, and

$$\mathbf{u}_2(z) = (z_\alpha - z)\nabla A + \frac{1}{2}\left(z_\alpha^2 - z^2\right)\nabla B \tag{2}$$

represents the depth-dependent correction at $O(\mu^2)$, with A and B given by

$$\begin{aligned} A &= \nabla \cdot (h\mathbf{u}_\alpha) \\ B &= \nabla \cdot \mathbf{u}_\alpha \end{aligned} \tag{3}$$

The derivation follows Chen (2006) except for the additional effect of letting the reference elevation z_α vary in time according to

$$z_\alpha = \zeta h + \beta \eta \tag{4}$$

where h is local still water depth, η is local surface displacement and ζ and β are constants, as in Kennedy et al (2001). This addition does not alter the details of the derivation, which are omitted below.

2.1 Governing equations

The equations of Chen (2006) extended to incorporate a possible moving reference elevation follow. The depth-integrated volume conservation equation is given by

$$\eta_t + \nabla \cdot \mathbf{M} = 0 \tag{5}$$

where

$$\mathbf{M} = H\left\{\mathbf{u}_\alpha + \overline{\mathbf{u}}_2\right\} \tag{6}$$

is the horizontal volume flux. $H = h + \eta$ is the total local water depth and $\overline{\mathbf{u}}_2$ is the depth averaged $O(\mu^2)$ contribution to the horizontal velocity field, given by

$$\overline{\mathbf{u}}_2 = \frac{1}{H}\int_{-h}^{\eta} \mathbf{u}_2(z)dz = \left(\frac{z_\alpha^2}{2} - \frac{1}{6}(h^2 - h\eta + \eta^2)\right)\nabla B + \left(z_\alpha + \frac{1}{2}(h-\eta)\right)\nabla A \tag{7}$$

The depth-averaged horizontal momentum equation can be written as

$$\mathbf{u}_{\alpha,t} + (\mathbf{u}_\alpha \cdot \nabla)\mathbf{u}_\alpha + g\nabla\eta + \mathbf{V}_1 + \mathbf{V}_2 + \mathbf{V}_3 + \mathbf{R} = 0 \tag{8}$$

where g is the gravitational acceleration and $\mathbf{R}$ represents diffusive and dissipative terms including bottom friction and subgrid lateral turbulent mixing. $\mathbf{V}_1$ and $\mathbf{V}_2$ are terms representing the dispersive Boussinesq terms given by

$$\mathbf{V}_1 = \left\{\frac{z_\alpha^2}{2}\nabla B + z_\alpha \nabla A\right\}_t - \nabla\left[\frac{\eta^2}{2}B_t + \eta A_t\right] \tag{9}$$

$$\mathbf{V}_2 = \nabla\left\{(z_\alpha - \eta)(\mathbf{u}_\alpha \cdot \nabla)A + \frac{1}{2}(z_\alpha^2 - \eta^2)(\mathbf{u}_\alpha \cdot \nabla)B + \frac{1}{2}[A + \eta B]^2\right\} \tag{10}$$

The form of (9) allows for the reference level z_α to be treated as a time-varying elevation, as suggested in Kennedy et al (2001). If this extension is neglected, the term reduces to the form

given originally by Wei et al (1995). The expression (10) for $\mathbf{V}_2$ was also given by Wei et al (1995), and is not altered by the choice of a fixed or moving reference elevation.

The term $\mathbf{V}_3$ in (8) represents the $O(\mu^2)$ contribution to the expression for $\boldsymbol{\omega} \times \mathbf{u} = \omega \mathbf{i}^z \times \mathbf{u}$ (where $\boldsymbol{\omega}$ is vorticity and with $\mathbf{i}^z$ the unit vector in the z direction) and may be written as

$$\mathbf{V}_3 = \omega_0 \mathbf{i}^z \times \overline{\mathbf{u}}_2 + \omega_2 \mathbf{i}^z \times \mathbf{u}_\alpha \tag{11}$$

where

$$\omega_0 = (\nabla \times \mathbf{u}_\alpha) \cdot \mathbf{i}^z = v_{\alpha,x} - u_{\alpha,y} \tag{12}$$

$$\omega_2 = (\nabla \times \overline{\mathbf{u}}_2) \cdot \mathbf{i}^z = z_{\alpha,x}(A_y + z_\alpha B_y) - z_{\alpha,y}(A_x + z_\alpha B_x) \tag{13}$$

Following Nwogu (1993), z_α is usually chosen in order to optimize the apparent dispersion relation of the linearized model relative to the full linear dispersion in some sense. In particular, the choice $\alpha = (z_\alpha/h)^2/2 + z_\alpha/h = -2/5$ recovers a Padé approximant form of the dispersion relation, while the choice $\alpha = -0.39$, corresponding to the choice $z_\alpha = -0.53h$, minimizes the maximum error in wave phase speed occurring over the range $0 \leq kh \leq \pi$. Kennedy et al (2001) showed that allowing z_α to move up and down with the passage of the wave field allowed a greater degree of flexibility in optimizing nonlinear behavior of the resulting model equations. In the examples chosen here, where a great deal of our focus is on the behavior of the model from the break point landward, we adopt Kennedy et al's "datum invariant" form

$$z_\alpha = -h + \beta H = (\beta - 1)h + \beta\eta = \zeta h + (1 + \zeta)\eta \tag{14}$$

with $\zeta = -0.53$ as in Nwogu (1993) and $\beta = 1 + \zeta = 0.47$. This corresponds in essence to a σ coordinate approach which places the reference elevation at a fixed level 53% of the total local depth below the local water surface. This also serves to keep the model reference elevation within the actual water column over the entire wetted extent of the model domain.

2.2 Treatment of the surface gradient term

The hybrid numerical scheme requires a conservative form of continuity equation and momentum equations, thus requiring a modification of the leading order pressure term in the momentum equation. A numerical imbalance problem occurs when the surface gradient term is conventionally split into an artificial flux gradient and a source term that includes the effect of the bed slope for a non-uniform bed. To eliminate errors introduced by the traditional depth gradient method (DGM), a so-called surface gradient method (SGM) proposed by Zhou et al. (2001) was adopted in the TVD based-Boussinesq models in the recent literature. Zhou et al. discussed an example of SGM in 1-D and verified that the slope-source term may be canceled out by part of the numerical flux term associated with water depth, if the bottom elevation at the cell center is constructed using the average of bottom elevations at two cell interfaces. Zhou et al. also showed a 2D application but without explicitly describing 2D numerical schemes. Although this scheme can be extended into

2D following the same procedure as in 1D, it was found that the 2D extension may not be trivial in terms of the bottom construction for a 2D arbitrary bathymetry. Kim et al. (2008) pointed out that the water depth in the slope-source term should be written in a discretized form rather than the value obtained using the bottom construction, implying that their revised SGM is valid for general 2D applications.

For the higher-order schemes such as the fourth-order TVD-MUSCL scheme (Yamamoto and Daiguji, 1993; Yamamoto et al., 1998) used in the recent Boussinesq applications, the original SGM and the revised SGM may not be effective in removing the artificial source. This problem was noticed by some recent authors such as Roeber et al. (2010) who kept a first-order scheme (second-order for normal conditions) for the numerical flux term and the slope-source term in order to ensure well-balanced solution without adding noise for a rapidly varying bathymetry.

In fact, the imbalance problem can be solved by a reformulation of this term in terms of deviations away from an unforced but separately specified equilibrium state (see general derivations in Rogers et al., 2003 and recent application in Liang and Marche, 2009). Using this technique, the surface gradient term may be split into

$$gH\nabla\eta = \nabla\left[\frac{1}{2}g(\eta^2 + 2h\eta)\right] - g\eta\nabla h \tag{15}$$

which is well-balanced for any numerical order under an unforced stationary condition (still water condition).

2.3 Conservative form of fully nonlinear Boussinesq equations

For Chen's (2006) equations or the minor extension considered here, $H\mathbf{u}_\alpha$ can be used as a conserved variable in the construction of a conservative form of Boussinesq equations, but resulting in a source term in the mass conservation equation such as in Shiach and Mingham (2009) and Roeber et al. (2010). An alternative approach is to use $\mathbf{M}$ as a conserved variable in terms of the physical meaning of mass conservation. In this study, we used $\mathbf{M}$, instead of $H\mathbf{u}_\alpha$, in the following derivations of the conservative form of the fully nonlinear Boussinesq equations.

Using M from (6) together with the vector identity

$$\nabla\cdot(\mathbf{uv}) = \nabla\mathbf{u}\cdot\mathbf{v} + (\nabla\cdot\mathbf{v})\mathbf{u} \tag{16}$$

allows (8) to be rearranged as

$$\begin{aligned}&\mathbf{M}_t + \nabla\cdot\left(\frac{\mathbf{MM}}{H}\right) + gH\nabla\eta \\ &= H\left\{\overline{\mathbf{u}}_{2,t} + \mathbf{u}_\alpha\cdot\nabla\overline{\mathbf{u}}_2 + \overline{\mathbf{u}}_2\cdot\nabla\mathbf{u}_\alpha - \mathbf{V}_1 - \mathbf{V}_2 - \mathbf{V}_3 - R\right\}\end{aligned} \tag{17}$$

Following Wei et al. (1995), we separate the time derivative dispersion terms in $\mathbf{V}_1$ according to

$$\mathbf{V}_1 = \mathbf{V}'_{1,t} + \mathbf{V}''_1 \tag{18}$$

where

$$\mathbf{V}_1' = \frac{z_\alpha^2}{2}\nabla B + z_\alpha \nabla A - \nabla\left[\frac{\eta^2}{2}B + \eta A\right] \tag{19}$$

and

$$\mathbf{V}_1'' = \nabla\left[\eta_t(A + \eta B)\right] \tag{20}$$

Using (15), (19) and (20), the momentum equation can be rewritten as

$$\begin{aligned} &\mathbf{M}_t + \nabla\cdot\left[\frac{\mathbf{MM}}{H}\right] + \nabla\left[\frac{1}{2}g(\eta^2 + 2h\eta)\right] = \\ &= H\left\{\overline{\mathbf{u}}_{2,t} + \mathbf{u}_\alpha\cdot\nabla\overline{\mathbf{u}}_2 + \overline{\mathbf{u}}_2\cdot\nabla\mathbf{u}_\alpha - \mathbf{V}_{1,t}' - \mathbf{V}_1'' - \mathbf{V}_2 - \mathbf{V}_3 - \mathbf{R}\right\} + g\eta\nabla h \end{aligned} \tag{21}$$

A difficulty usually arises in applying the adaptive time-stepping scheme to the time derivative dispersive terms $\bar{u}_{2,t}$ and $\mathbf{V}_{1,t}'$ which are usually calculated using values stored in several time levels in the previous Boussinesq codes such as in Wei et al. (1995) and Shi et al. (2001). The equation can be re-arranged by merging the time derivatives on the right hand side into the time derivative term on the left hand side, giving

$$\begin{aligned} \mathbf{V}_t \quad &+\nabla\cdot\left[\frac{\mathbf{MM}}{H}\right] + \nabla\left[\frac{1}{2}g(\eta^2 + 2h\eta)\right] = \eta_t(\mathbf{V}_1' - \overline{\mathbf{u}}_2) \\ &+H\left(\mathbf{u}_\alpha\cdot\overline{\mathbf{u}}_2 + \overline{\mathbf{u}}_2\cdot\nabla\mathbf{u}_\alpha - \mathbf{V}_1'' - \mathbf{V}_2 - \mathbf{V}_3 - \mathbf{R}\right) + g\eta\nabla h \end{aligned} \tag{22}$$

where

$$\mathbf{V} = H(\mathbf{u}_\alpha + \mathbf{V}_1') \tag{23}$$

In (23), η_t can be calculated explicitly using (5) as in Roeber et al. (2010). Equations (5) and (22) are the governing equations solved in FUNWAVE-TVD. After $\mathbf{V}$ is obtained, the velocity $\mathbf{u}_\alpha$ can be solved by a system of tridiagonal matrix equation formed by (23) in which all cross-derivatives are moved to the right-hand side of the equation.

2.4 Numerical schemes

The governing equations in FUNWAVE-TVD are discretized on a regular grid using a hybrid finite-volume / finite-difference approach. The numerical scheme is described in detail in Shi et al (2011a, 2011b) and is omitted here for conciseness. Examples described below are based on discretizations on regular Cartesian grids with uniform grid spacings in x and y. Terms in conservative form in equations (5) and (22) are written in finite volume form using a MUSCL-TVD scheme, while additional terms are written in cell-centered finite differences. An adaptive third-order Strong Stability Preserving (SSP) Runge-Kutta scheme is used for time stepping (Gottlieb et al, 2001).

2.5 Wave breaking and wetting-drying schemes for shallow water

The wave breaking scheme follows the approach of Tonelli and Petti (2009) who successfully used the ability of NSWE with a TVD scheme to model moving hydraulic jumps. The fully nonlinear Boussinesq equations are switched to NSWE at cells where the Froude number exceeds an certain threshold. The threshold value is set to be 0.8 as suggested by Tonelli and Petti.

The wetting-drying scheme for modeling of a moving boundary is straightforward. The normal flux $\mathbf{n} \cdot \mathbf{M}$ at the cell interface of a dry cell is set to zero. A mirror boundary condition is applied to the MUSCL-TVD scheme and discretization of dispersive terms at dry cells.

2.6 Boundary conditions and wavemaker

We implemented various boundary conditions including wall boundary condition, absorbing boundary condition following Kirby et al. (1998) and periodic boundary condition following Chen et al. (2003).

Wavemakers implemented in the study include Wei et al's (1999) internal wavemakers for regular waves and irregular waves. For the irregular wavemaker, an extension was made to incorporate the alongshore periodicity into wave generation in order to eliminate a boundary effect on wave simulation. The technique exactly follows the strategy in Chen et al. (2003) who adjusted the distribution of wave directions in each frequency bin to obtain alongshore periodicity. This approach is effective in modeling of breaking wave-induced nearshore circulation such as alongshore currents and rip currents.

2.7 Parallelization

In parallelizing the computational model, we use the domain decomposition technique to subdivide the problem into multiple regions and assign each subdomain to a separate processor core. Each subdomain region contains an overlapping area of ghost cells three rows deep, as dictated by the MUSCL-TVD scheme. The Message Passing Interface (MPI) with non-blocking communication is used to exchange the data in the overlapping region between neighboring processors. Velocity components are obtained from Equation (23) by solving tridiagonal matrices using the parallel pipelining tridiagonal solver described in Naik et al. (1993).

3 Basic hydrodynamic considerations

There are two basic states which are required in ensuring that any numerical model works for predicting evolution and inundations. The first step is to ensuring that the model conserves mass; the second basic step is checking convergence of this numerical code to a asymptotic limit.

	Maximum Runup		
Grid Size	$H/d = 0.045$	$H/d = 0.091$	$H/d = 0.181$
0.1	0.02302	0.04061	0.06311
0.05	0.02303	0.04063	0.06315
0.01	0.02303	0.04064	0.06316
0.005	0.02303	0.04064	0.06316

Table 1: Maximum runup for gauge 9 for different grid size.

3.1 Mass conservation

Conservation of mass can be checked by calculating water volume at the beginning and at the end of the computation. This should be dine by integrating disturbed water depth $\eta(x, y, t)$ over the entire flow domain, i.e., if the flow domain extends from the maximum penetration during inundation $x = X_{max}$ to the outer location of the source region X_S, and $y = Y_{max}$ to Y_s, then the total displaced volume $V(t)$ is,

$$V(t) = \int_{X_{max}}^{X_S} \int_{Y_{max}}^{Y_S} \eta(x, y, t) dx dy \tag{24}$$

The integral of $\eta(x, y, t)$ should be used instead of the integral of the entire flow depth $h(x, y, t) = \eta(x, y, t) + d(x, y, t)$ where $d(x, y, t)$ is the undisturbed water depth, because the latter is likely to conceal errors in the calculation. Typically,$\eta << d$ at offshore integrating h will simply produce the entire volume of the flow domain and will mask errors. Note that testing of the conservation of mass as above involves placing a closed domain within reflective boundaries (Synolakis et al., 2007).

Calculations of conservation of mass has been done for all of the benchmark problems reviewed in this report such that the total initial displaced volume $V(t = 0)$ was within less than 1% of the total displaced volume at the end of the computation $V(t = T)$ where T represents the computation end time. It is assumed that the end of the computation is when the initial wave is entirely reflected and reached offshore. However, with few changes in Δx and Δy the conservation of mass can be improved.

3.2 Convergence

Convergence is the another basic hydrodynamic consideration that is checked for all of the benchmarks in this research. Actually this process is made by checking convergence of the numerical code to a certain asymptotic limit, presumably the actual solution of the equations solved. The grid steps Δx and Δy has been halved, and the time step Δt automatically reduced appropriately

to conform to the Courant-Friedrics-Levy (CFL) criterion. As recommended in literature, convergence of the code has been checked through the extreme runup and rundown. Table 1 displays convergence of the code tested during the conical island test problem which is discussed in Section 5.3 below.

4 Analytical benchmarks

In this section, using analytical description of shallow water-wave (SW) equations for evolution of the water surface, numerical results for different test cases is compared analytical solution. Also, in this section we present several analytic solutions to the 1+1 version of shallow water-wave (SW) equations. Although 1+1 models are not completely reliable for estimation of tsunmi behaviour such as inundation mapping, they are first step of testing and validating models (Synolakis et al., 2007).

In this section following benchmark problems has been studied:

1. Solitary wave on a simple beach
2. N-wave on a simple beach
3. Solitary wave on a composite beach

4.1 Solitary wave on a simple beach

The canonical problem of the shallow water-wave equations is covered here which contains the calculation of a long wave climbing up a sloping beach of angle β attached to a constant-depth region (Figure 1). The origin of the coordinate system is at the initial position of the shoreline and x increases seaward.

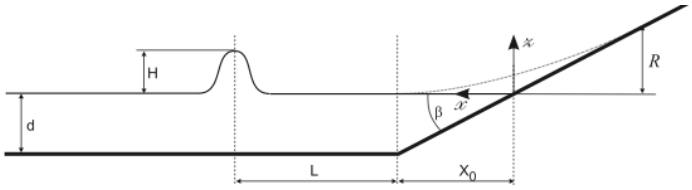

Figure 1: Definition sketch for simple beach bathymetry(from Synolakis et al (2007, Figure A1)).

It is possible to derive exact results for the evolution and runup of solitary waves based on linear theory (Synolakis, 1986, 1987). Solitary waves have long been used as a model for the leading wave of tsunamis. Russell (1845) defined solitary waves as the great waves of translation, and consists of a single elevation wave. While capturing some of the basic physics of tsunamis, solitary waves do not model the physical manifestation of tsunamis in nature, which are invariably N-wave like with

				R/d		
d(m)	$\Delta x(m)$	H/d	$Cot(\beta)$	Runup Law	Numerical Calculations	Error(%)
0.5	0.1	0.03	10.0	0.112	0.110	1.6
0.5	0.1	0.05	10.0	0.212	0.204	3.6
0.5	0.1	0.1	3.333	0.291	0.282	3.0
0.5	0.1	0.48	1.0	1.131	1.109	2.0
0.5	0.1	0.01	20.0	0.040	0.042	4.9
5.0	1.0	0.03	10.0	0.112	0.112	0.4
5.0	1.0	0.05	10.0	0.212	0.212	0.2
5.0	1.0	0.10	3.372	0.308	0.315	2.4
5.0	1.0	0.10	3.372	0.731	0.734	0.3
5.0	1.0	0.294	2.747	1.016	1.058	4.2
5.0	1.0	0.005	20.0	0.017	0.017	1.1
5.0	1.0	0.01	20.0	0.040	0.039	3.0
100	5.0	0.05	10.0	0.212	0.202	4.5
100	5.0	0.03	2.747	0.257	0.266	3.4
100	5.0	0.03	2.747	0.600	0.598	0.4
100	5.0	0.03	20.0	0.040	0.040	0.2

Table 2: Runup data from numerical calculations compared with runup law values.

a leading-depression wave followed by an elevation wave (Synolakis et al., 2007). The following runup law for the maximum runup R is provided based on slope of the beach and wave height of the solitary wave

$$R = 2.831\sqrt{\cot\beta}H^{\frac{5}{4}} \tag{25}$$

Benchmark problems that are studied here have different depths from 50cm to 1000m. Also, for each depth, different slopes and wave heights has been studied. Table 2 provides a list of selected examples that has been modeled including their maximum runup and the grid size for each case. Figure 2 defines a comparison between numerical simulation and runup law.

In addition, the analytical solution for different times is available for a specific case in which $H/d = 0.0019$ and $\beta = \text{arccot}(19.85)$. In order to have the same time with the data it was recommended that $L = \text{arccosh}(\sqrt{20})/\gamma$ in which $\gamma = \sqrt{3H/4d}$; therefore, the distance of the wave from initial shoreline(X_1) can be written as $X_1 = X_0 + L$ (with respect to Figure 1). Figure 3 demonstrates profiles and time series of the water in eight different times. Extreme positions of the shoreline are shown in figure 3 (the maximum runup and rundown occur $t \simeq 55(d/g)^{1/2}$ and $t \simeq 70(d/g)^{1/2}$). Figure 4 shows water level fluctuations at two gauge locations $X/d = 0.25$, $X/d = 9.95$. As it is clear in the figure the point $X/d = 0.25$ which is closer to initial shoreline, becomes temporarily dry during the process but the point $X/d = 9.95$ remains wet throughout the

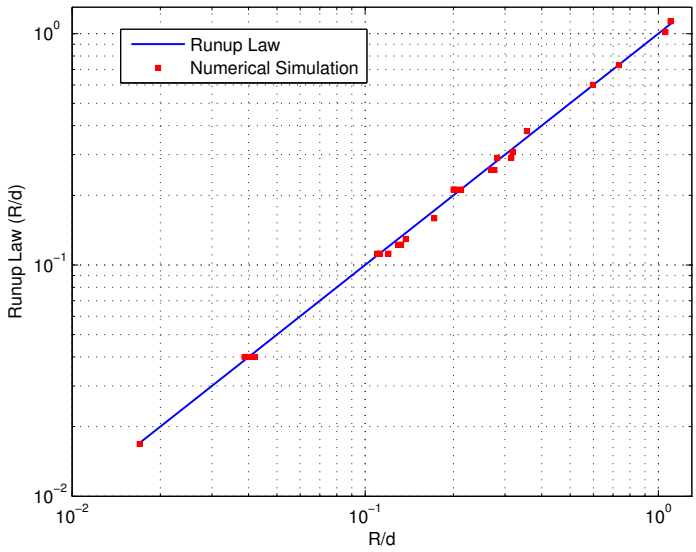

Figure 2: Numerical simulation data for maximum runup of nonbreaking waves climbing up different beach slopes. Solid line represents the runup law (25).

entire length of the numerical simulation.

4.2 N-wave runup on a simple beach

Most tsunami eyewitness accounts suggest that tsunamis are N-wave like, i.e., they are dipolar, which means they appear as a combination of a depression and an elevation wave, and frequently as a series of N-waves, sometimes known as double N-waves (Synolakis et al., 2007).

Tadepalli and Synolakis (1994) described an N-wave with leading-elevation and depression waves of the same height and at a constant separation distance and refer to this wave as an isosceles N-wave with a surface profile given by

$$\eta(x,0) = \frac{3\sqrt{3}H}{2}\mathrm{sech}^2[\gamma(x-X_N)]\tanh[\gamma(x-X_N)] \tag{26}$$

where

$$\gamma = \frac{3}{2}\sqrt{\sqrt{\frac{3}{4}}H} \tag{27}$$

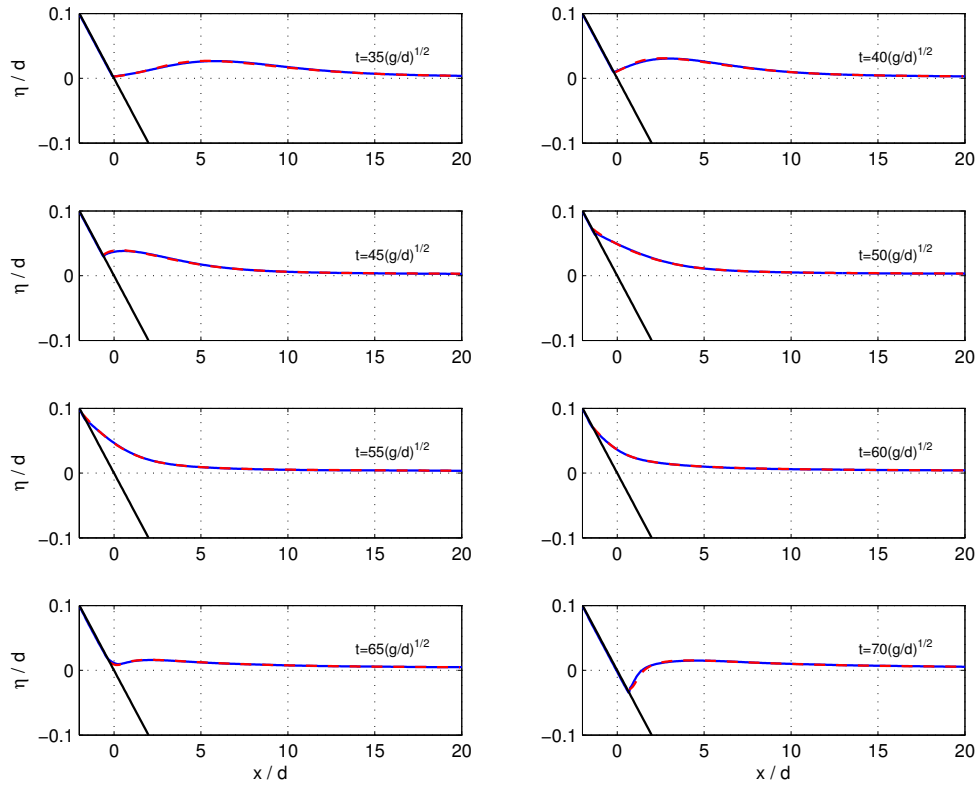

Figure 3: The water level profiles during runup of the non-breaking wave in the case of $H/d = 0.019$ on a 1:19.85 beach. Solid blue line represents the analytical solution in according to Synolakis(1986), and dashed red lines represents the numerical simulation.

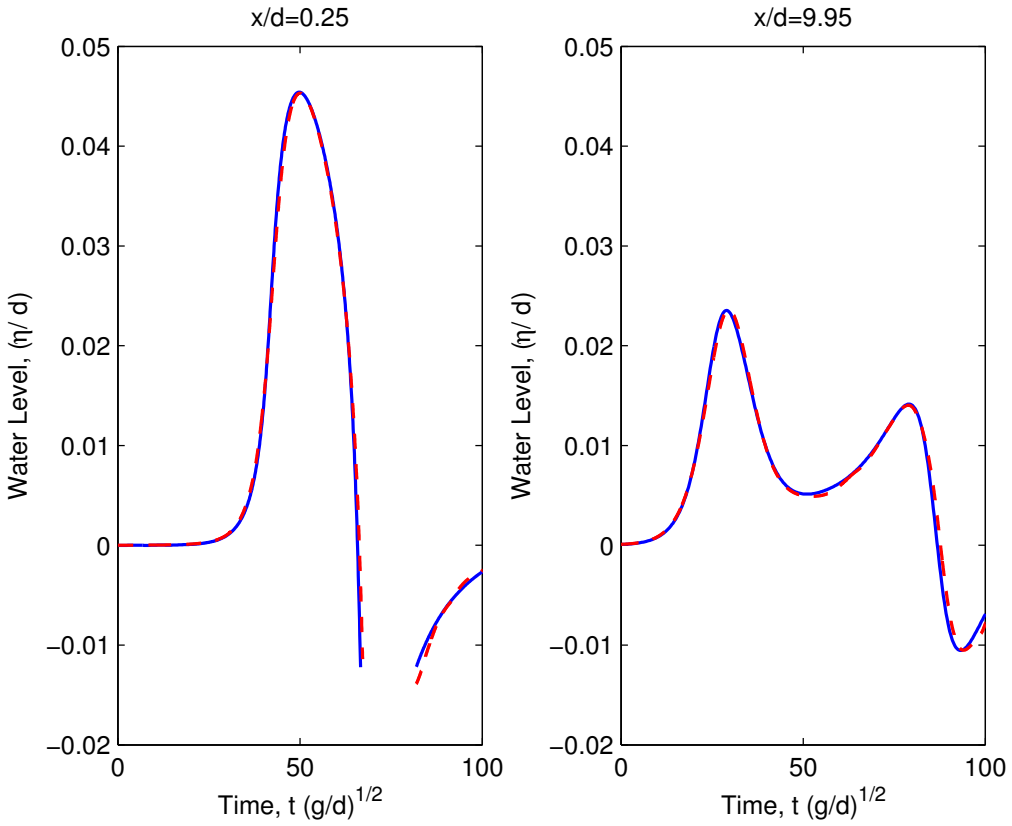

Figure 4: The water level dynamics at two locations $X/d = 0.25$ and $X/d = 9.95$. Solid blue line represents the analytical solution in according to Synolakis(1986), and dashed red line represents the numerical simulation.

					R/d		
d(m)	γ	Δx(m)	H/d	$\cot(\beta)$	Runup Law	Numerical Calculations	Error (%)
0.5	0.22	0.1	0.05	3.333	0.167	0.165	1.0
0.5	0.44	0.1	0.2	1.0	0.516	0.505	2.2
5.0	0.54	1.0	0.03	10.0	0.152	0.157	3.0
5.0	0.70	1.0	0.05	10.0	0.289	0.286	0.9
5.0	0.99	1.0	0.1	3.732	0.419	0.433	3.3
5.0	1.69	1.0	0.294	2.747	1.385	1.388	0.2
5.0	0.22	1.0	0.005	20.0	0.023	0.023	0.2
5.0	0.31	1.0	0.01	20.0	0.055	0.056	2.6
100.0	3.12	5.0	0.05	10.0	0.289	0.277	4.0
100.0	6.13	5.0	0.193	2.747	0.818	0.826	0.9
100.0	1.40	5.0	0.01	20.0	0.055	0.056	2.6
1000.0	9.87	20.0	0.05	10.0	0.289	0.275	4.7
1000.0	9.87	20.0	0.05	3.333	0.167	0.173	3.8

Table 3: Runup data from numerical calculations compared with runup law for N-wave.

Similar to previous part, following expression for the maximum runup of N-waves has been provided based on slope of the beach and wave height of the N-wave similar to solitary wave problem:

$$R = 3.86\sqrt{\cot\beta}H^{\frac{5}{4}} \tag{28}$$

Benchmark problems that are studied here have different depths from 50cm to 1000m. Also, for each depth different slope and wave heights has been studied. Table 3 provides a list of selected different cases that has been modeled including their maximum runup and the grid size for each case. Figure 5 defines a comparison between numerical simulation and runup law for N-wave problem.

4.3 Solitary wave on composite beach

In this benchmark problem a complex topography consisting of three segments and a vertical wall is considered (Figure 6). The benchmark test is described in Appendix A, Section 2.2 of Synolakis et al (2007). Runup of non-breaking solitary waves on the vertical wall is simulated in this case. Results have been compared with the analytical solution. Laboratory data exist for this topography from a U.S. Army Corps of Engineers, Coastal Engineering Research Center, Vicksburg, Mississippi experiment of wave runup on a model of Revere Beach, Massachusetts. However, the maximum runup for solitary waves propagating up Revere Beach (Composite Beach) is given by

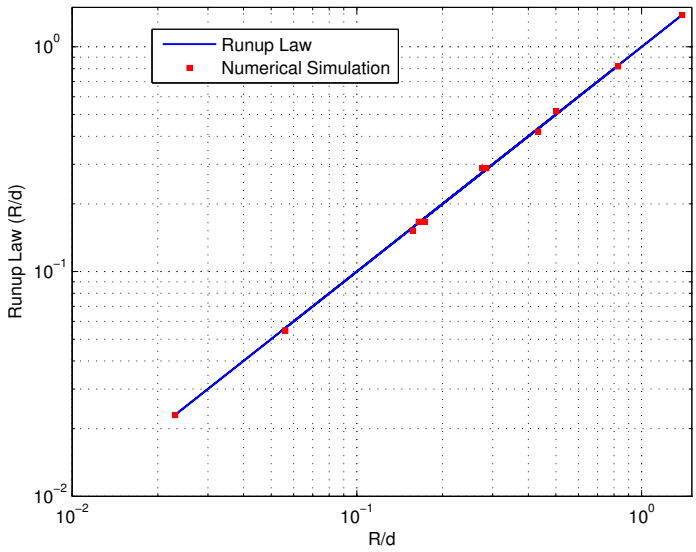

Figure 5: Numerical simulation data for maximum runup of N-waves climbing up different beach slopes. Solid line represents the runup law (28).

the runup law

$$R = 2h_w^{-\frac{1}{4}} H \tag{29}$$

where $h_w$is the initial depth at the right vertical wall and H is the solitary wave height.

Two initial depths have been studied here; $d = 18.8$ cm, and $d = 21.8$ cm. For all cases a grid size of $\Delta x = 0.10$m has been used. Table 4 demonstrates a comparison of runup law with the

$d = 21.8$ cm				$d = 18.8$ cm			
H(m)	R(Runup Law)	R(Numerical)	Error (%)	H(m)	R(Runup Law)	R(Numerical)	Error (%)
0.005	0.0146	0.0141	3.7	0.005	0.0152	0.0148	2.5
0.01	0.0293	0.0288	1.6	0.01	0.0304	0.0310	2.1
0.03	0.0878	0.0850	3.2	0.03	0.0911	0.0871	4.4
0.05	0.1463	0.1390	5.0	0.05	0.1519	0.1440	5.2

Table 4: Maximum runup of solitary wave on composite beach compared to runup law (29).

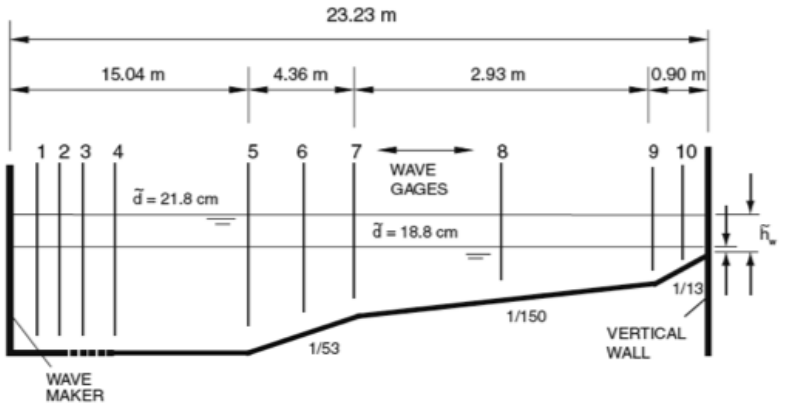

Figure 6: Definition sketch for Revere Beach (from Synolakis et al (2007, Figure A7)).

numerical data for both depths studied here.

In addition, for this benchmark problem three different waves have been modeled ($H/d = 0.0378, 0.2578, 0.6404$ for cases A, B and C). Recorded data is compared with the analytical data for gauge 4 to gauge 10 and also on the wall in Figures 7 - 9 . Grid size for this case is $\Delta x = 0.010$ m. It should be mentioned that for analytical results the model has been used in linear, non-dispersive and no friction mode.

5 Laboratory benchmarks

In this section different laboratory benchmarks are studied and result of numerical calculations is compared with the laboratory data. Following benchmark problems are studied in this section:

1. Solitary wave on a simple beach
2. Solitary wave on a composite beach
3. Solitary wave on a conical island
4. Tsunami runup onto a complex three-dimensional beach; Monai Valley

5.1 Solitary wave on a simple beach

In this laboratory test, the 31.73 m-long, 60.96 cm-deep and 39.97 cm wide California Institute of Technology, Pasadena, California wave tank was used with water at varying depths. The tank is

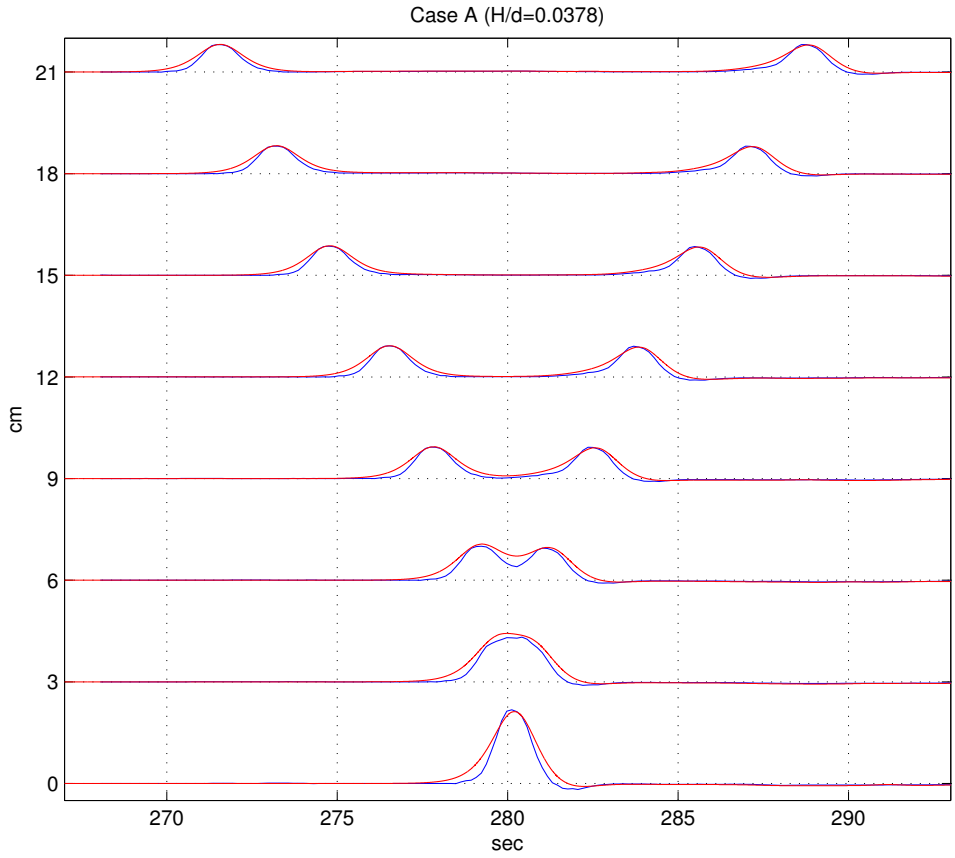

Figure 7: Time evolution of nonbreaking $H/d = 0.0378$ initial wave on composite beach. The red line shows the numerical solution and blue line represents the analytic solution.

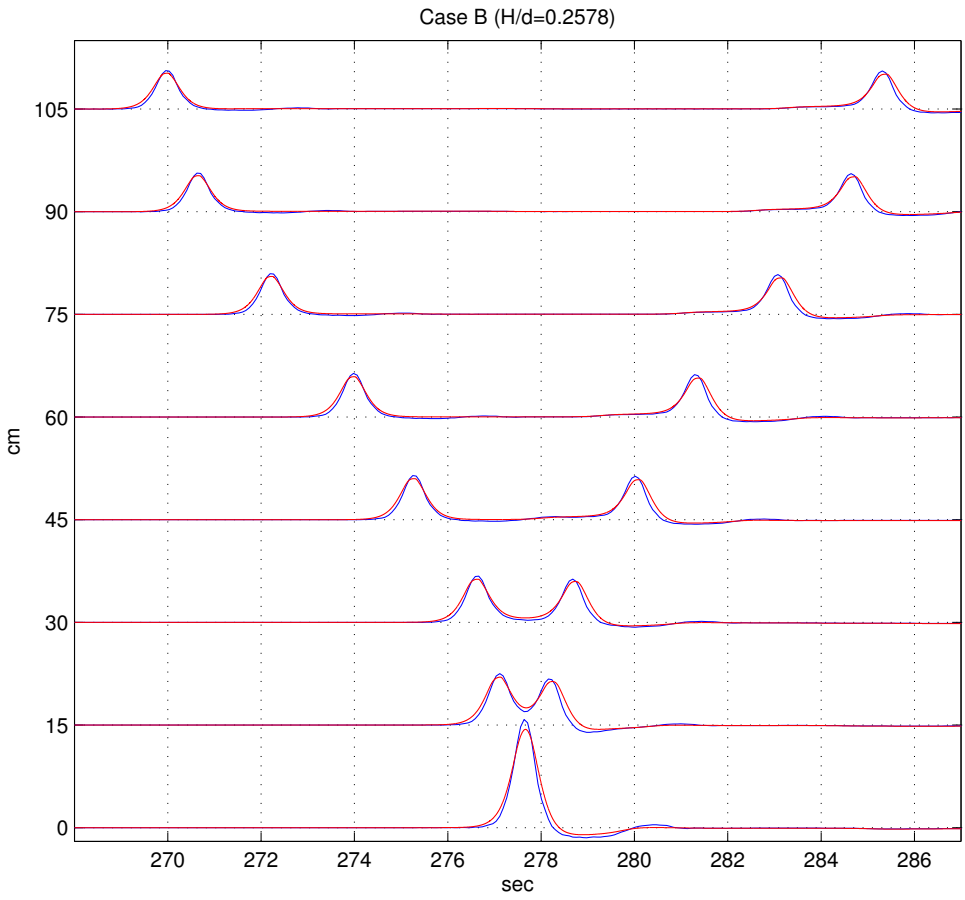

Figure 8: Time evolution of breaking $H/d = 0.2578$ initial wave on composite beach. The red line shows the numerical solution and blue line represents the analytic solution.

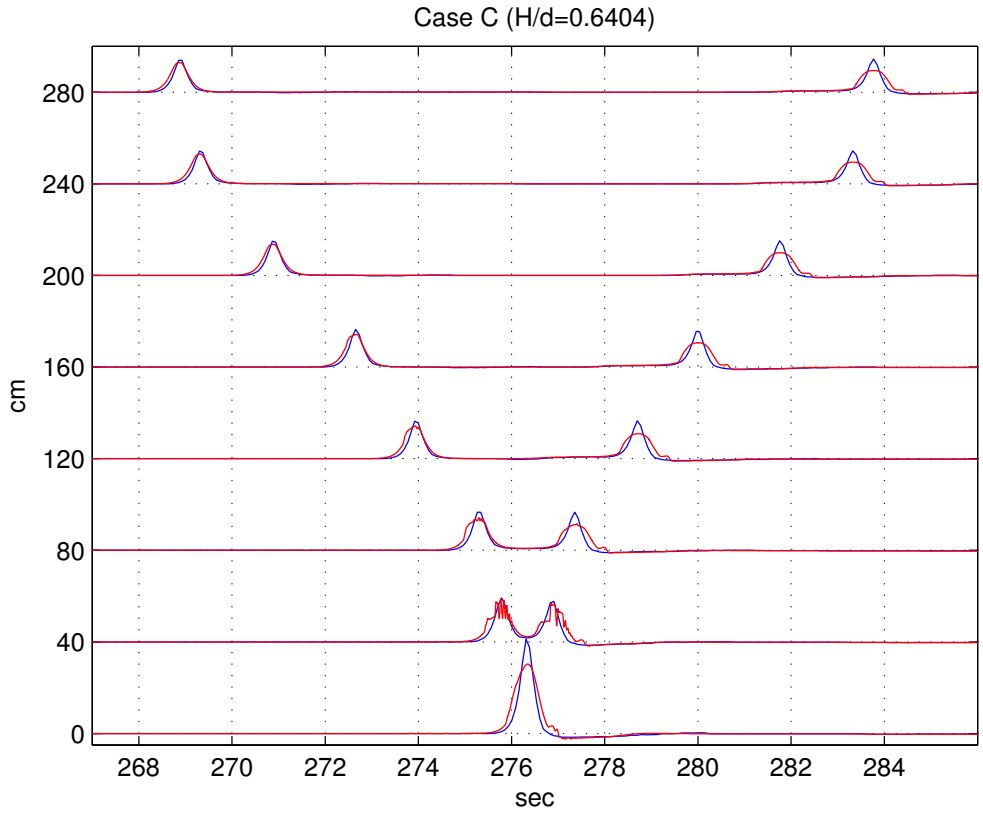

Figure 9: Time evolution of breaking $H/d = 0.6404$ initial wave on composite beach. The red line shows the numerical solution and blue line represents the analytic solution.

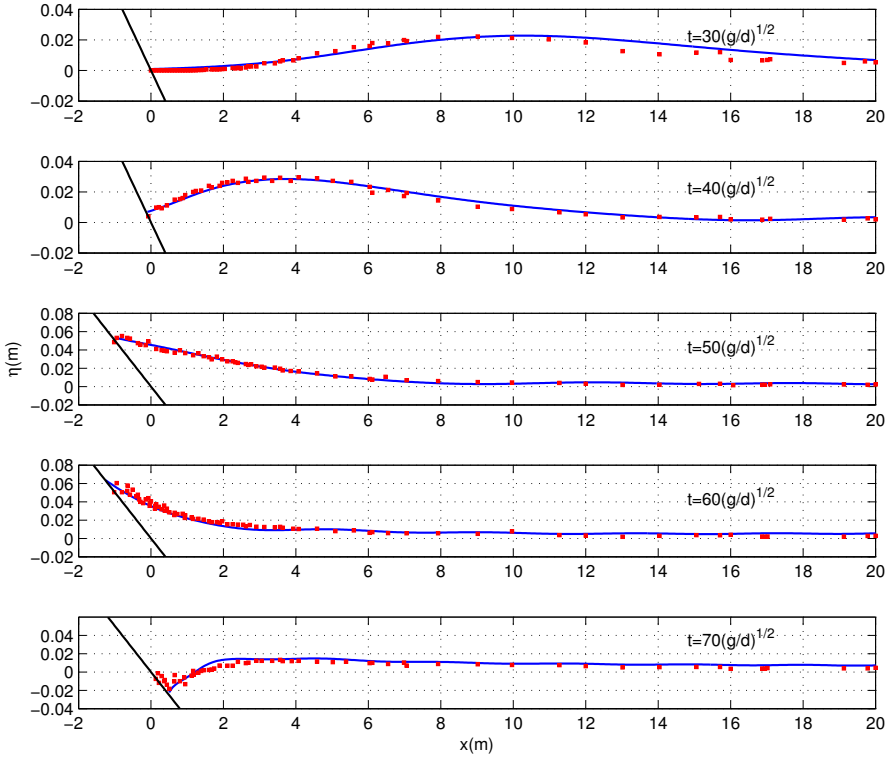

Figure 10: Time evolution of nonbreaking $H/d = 0.0185$ initial wave. The solid line shows the numerical solution and dots represent the laboratory data.

described by Synolakis (1986, 1987). The bottom of the tank consisted of painted stainless steel plates. A ramp was installed at one end of the tank to model the bathymetry of the canonical problem of a constant-depth region adjoining a sloping beach. The ramp had a slope of 1:19.85. The ramp was sealed to the tank side walls. The toe of the ramp was distant 14.95 m from the rest position of the piston generator used to generate waves.

This set of laboratory data has been vastly used for many code validations. In this modeling test, the data sets for the $\tilde{H}/\tilde{d} = 0.0185$ nonbreaking and $\tilde{H}/\tilde{d} = 0.30$ breaking solitary waves which are the most frequently used and most appropriate for code validation.

For these cases a grid size of $\Delta x = 0.10$ m has been used. Figure 10 and Figure 11 displays the accuracy of the model for both nonbreaking and breaking waves. The runup error for the

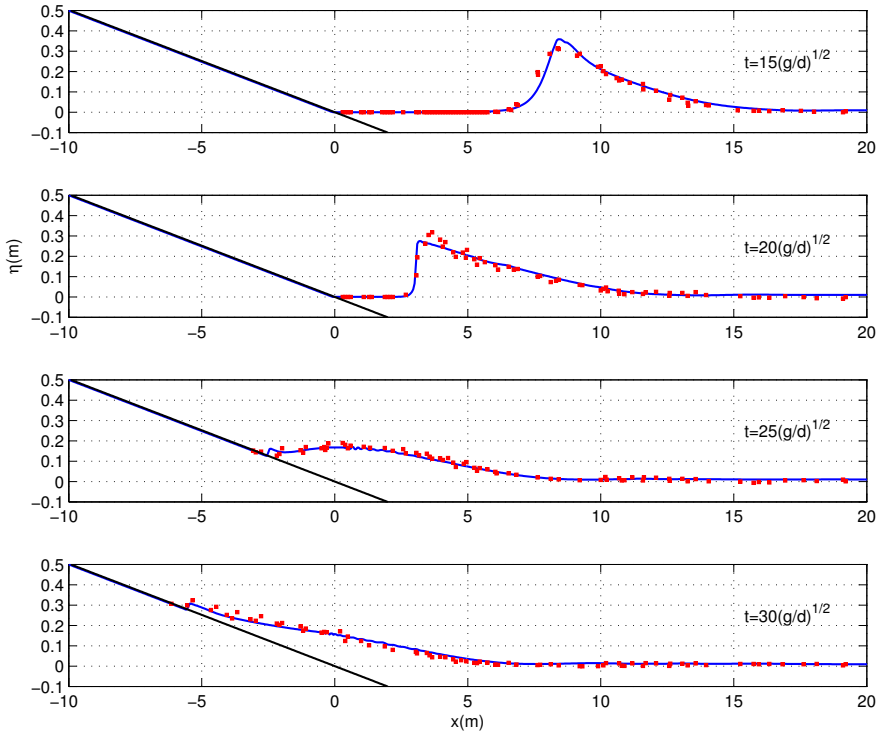

Figure 11: Time evolution of breaking $H/d = 0.3$ initial wave. The solid line shows the numerical solution and dots represent the laboratory data.

nonbreaking wave case was 3.3% and for the breaking wave was 5.8%.

5.2 Solitary wave on a composite beach

Revere Beach is located approximately 6 miles northeast of Boston in the City of Revere, Massachusetts. To address beach erosion and severe flooding problems, a physical model of the beach was constructed at the Coastal Engineering Laboratory of the U.S. Army Corps of Engineers, Vicksburg, Mississippi facility, earlier known as Coastal Engineering Research Center. This benchmark is described in Section 3.2 of Appendix A of Synolakis et al (2007).

The beach characteristics are exactly the same as the composite beach described in section 4.3. In this benchmark problem three different waves are modeled ($H/d = 0.0378, 0.2578, 0.6404$ for

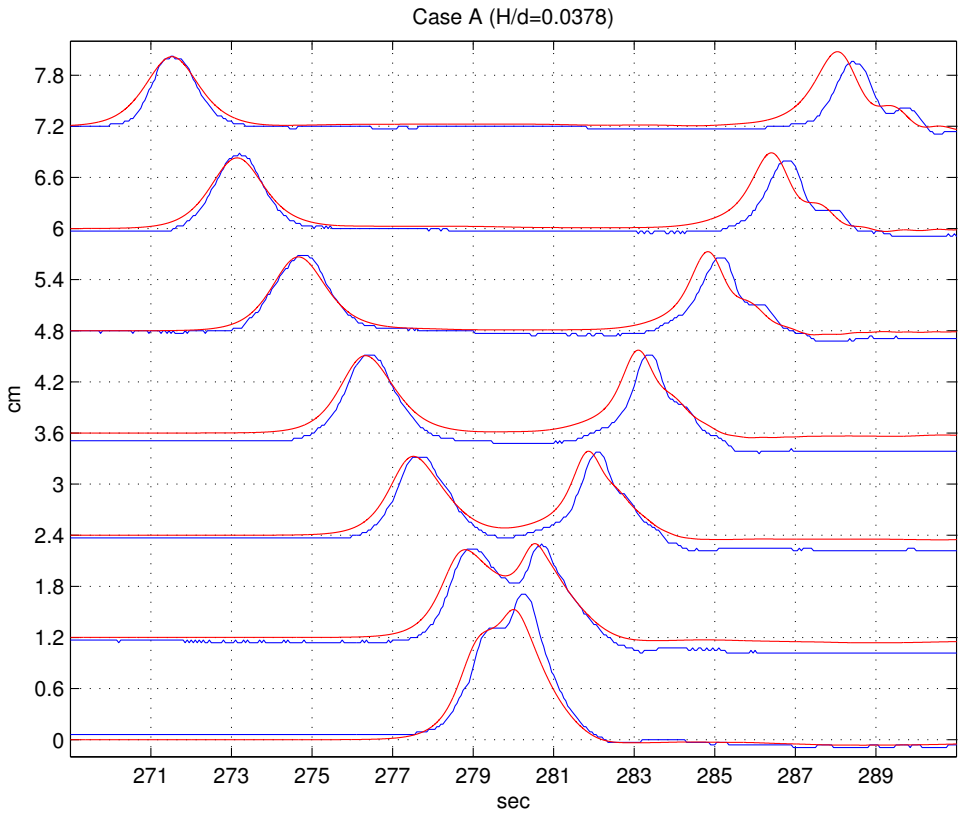

Figure 12: Time evolution of nonbreaking $H/d = 0.0378$ initial wave on composite beach. The red line shows the numerical solution and blue line represents the laboratory data.

cases A, B and C) and the numerical data is compared with the laboratory data for gauges 4 to 10 in Figures 12 - 14). Grid size for this case is $\Delta x = 0.010$ m.

5.3 Solitary wave on a conical island

Laboratory experiments on the interaction between solitary waves and a conical island were conducted by Briggs et al (1995). The three cases from this test illustrate the important fact that runup and inundation heights on the sheltered back sides of an island can exceed the incident wave height on the exposed front side, due to trapping of wave fronts propagating around the island circumference. These tests have been used in a number of validation studies for a variety of models,

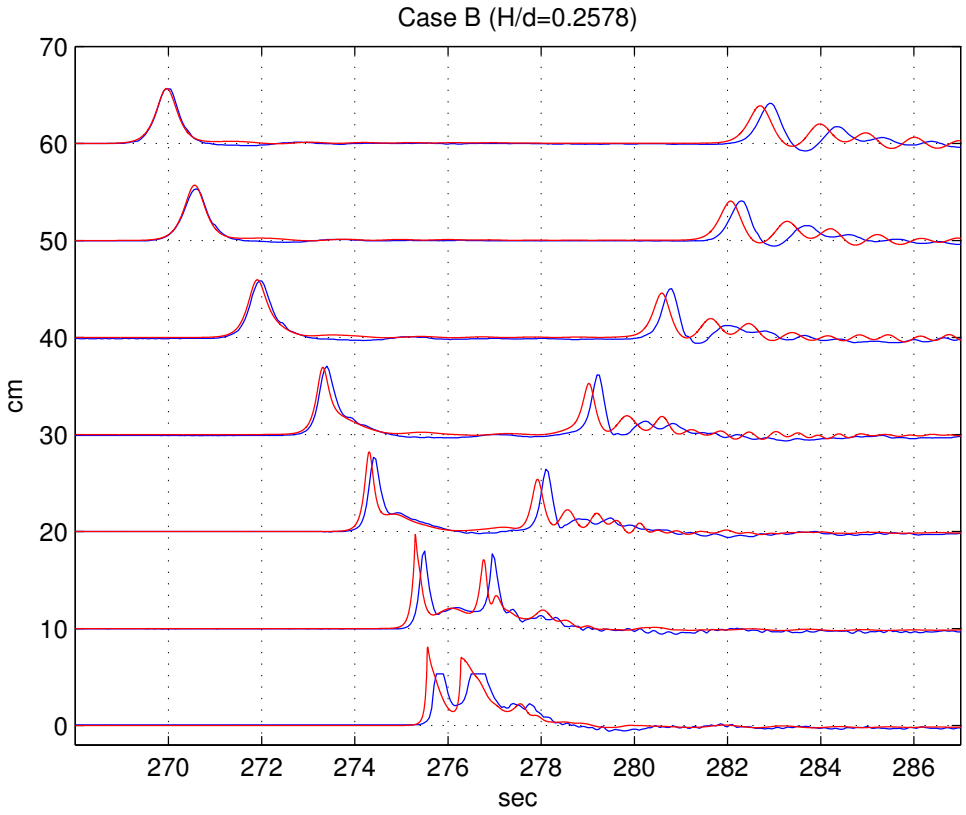

Figure 13: Time evolution of breaking $H/d = 0.2578$ initial wave on composite beach. The red line shows the numerical solution and blue line represents the laboratory data.

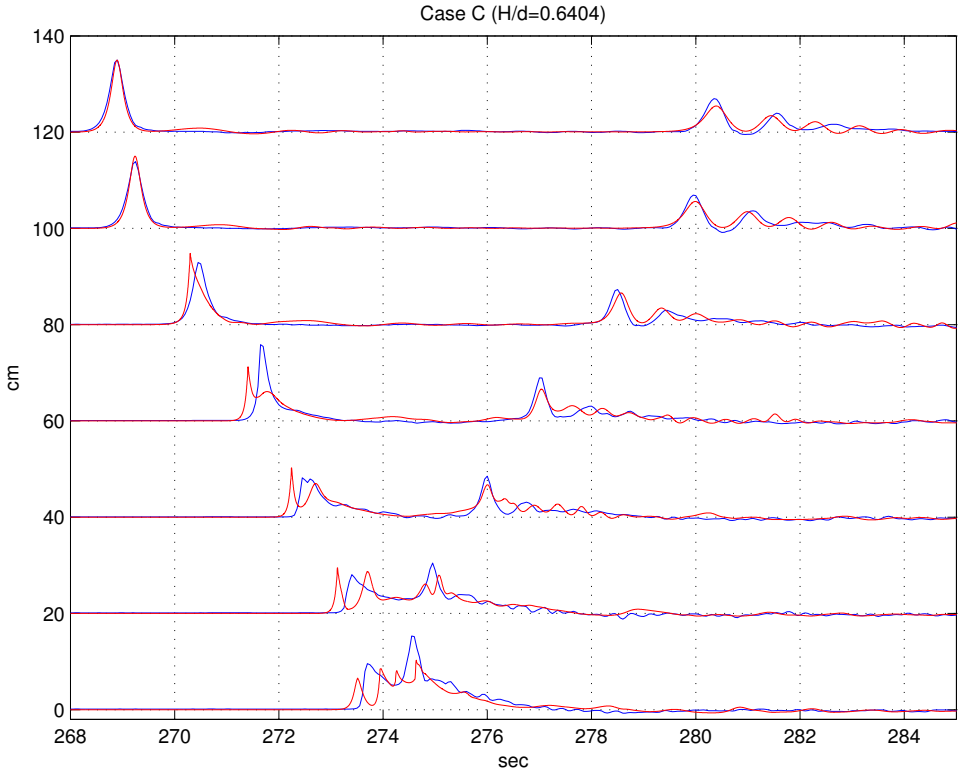

Figure 14: Time evolution of breaking $H/d = 0.6404$ initial wave on composite beach. The red line shows the numerical solution and blue line represents the laboratory data.

including nonlinear shallow water equations (Liu et al 1995) and Boussinesq equations (Chen et al, 2000). The benchmark test is specified in Section 3.3 of Appendix A of Synolakis et al (2007).

Large-scale laboratory experiments were performed at Coastal Engineering Research Center, Vicksburg, Mississippi, in a 30m-wide, 25m-long, and 60cm-deep wave basin (Figure 15). In the physical model, a 62.5cm-high, 7.2m toe-diameter, and 2.2m crest-diameter circular island with a 1:4 slope was located in the basin (Figure 16). Experiments were conducted at depth of 32cm, with three different solitary waves (H/d=0.045, 0.091, 0.181). Water-surface time histories were measured with 27 wave gages located around the perimeter of the island (Figure 17).

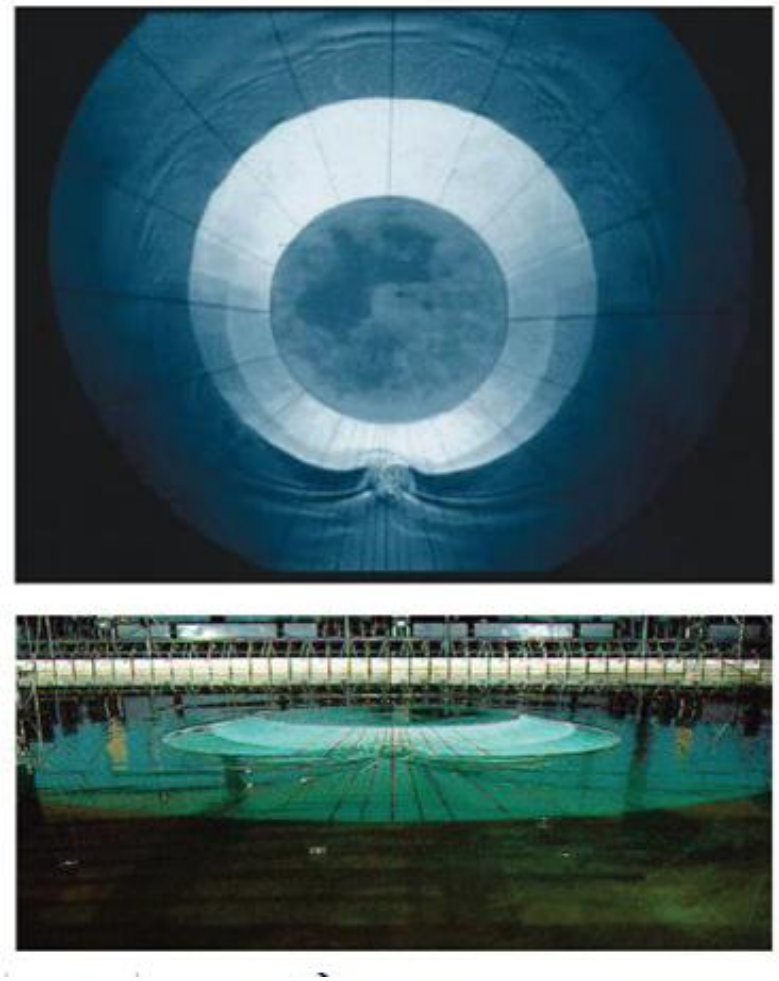

Figure 15: View of conical island(top) and basin(bottom)(from Synolakis et al (2007, Figure A16)).

For this benchmark test, time histories of the surface elevation around the circular island are given at four locations, i.e., in the front of the island at the toe (Gauge 6) and gauges closest to the

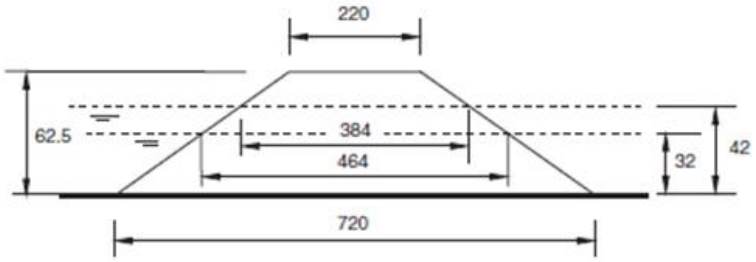

Figure 16: Definition sketch for conical island. All dimensions are in cm (from Synolakis et al (2007, Figure A17)).

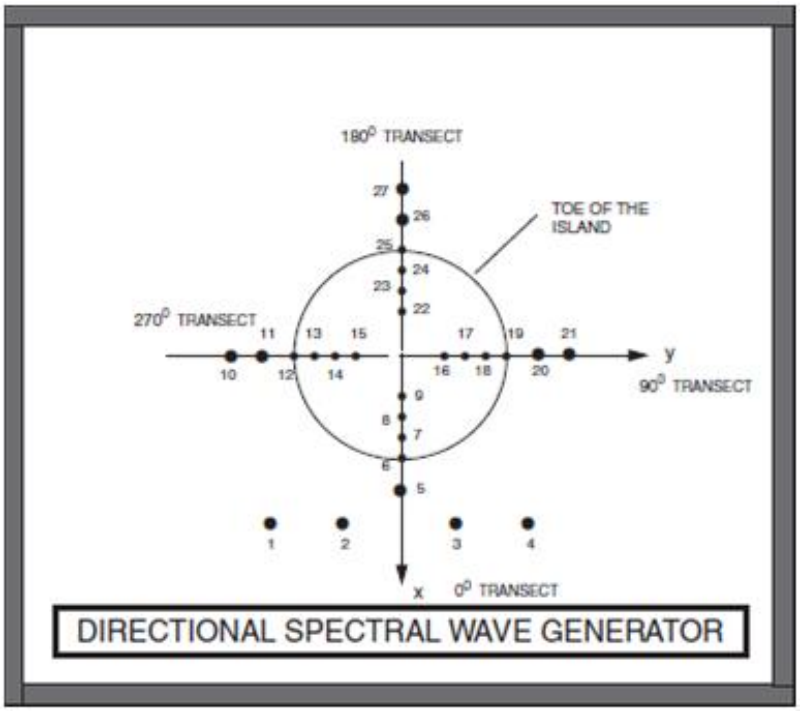

Figure 17: Schematic gauge locations around the conical island(from Synolakis et al (2007, Figure A18)).

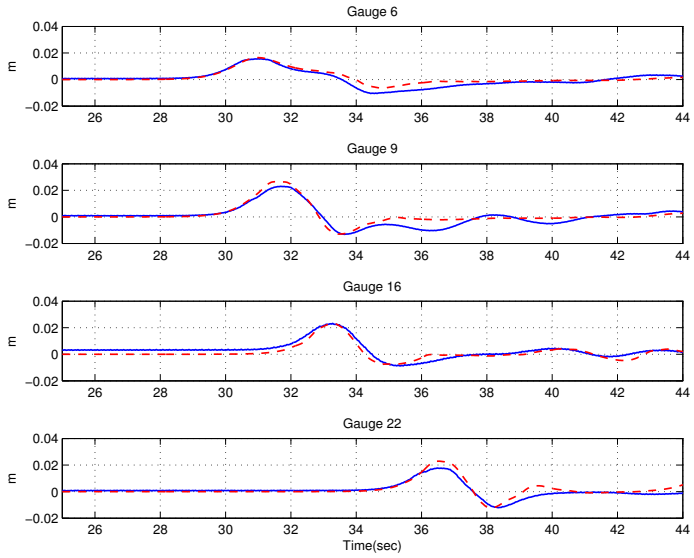

Figure 18: Comparison of computed and measured time series of free surface for $H/d = 0.045$.Solid lines: measured, Dashed lines: Computed.

shoreline with the numbers 9, 16, and 22 located at the 0°, 90°, and 180° radial lines (Figure 17). A grid size of $\Delta x = 0.10m$ is considered for proper numerical simulation of this benchmark. Figures 18-20 shows the comparison between the laboratory data with numerical calculations. Table 5 represents the error of the maximum runup for each gauge for different wave heights.

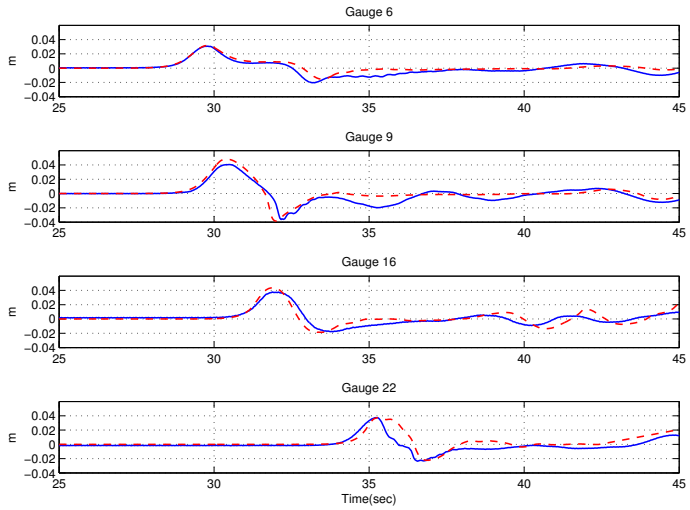

Figure 19: Comparison of computed and measured time series of free surface for $H/d = 0.091$.Solid lines: measured, Dashed lines: Computed.

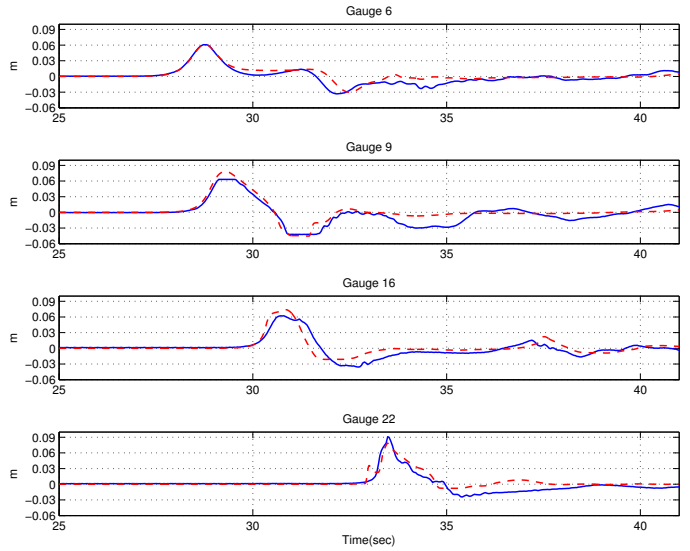

Figure 20: Comparison of computed and measured time series of free surface for $H/d = 0.181$.Solid lines: measured, Dashed lines: Computed.

	Gauge Number			
H/d	6	9	16	22
0.045	6.0	13.2	0.1	18.9
0.091	3.2	16.6	11.6	0.26
0.181	1.6	13.33	13.8	13.3

Table 5: Percent error of predicted maximum runup calculated for each gauge in conical island test.

5.4 Tsunami runup onto a complex three-dimensional beach; Monai Valley

The Hokkaido-Nansei-Oki tsunami of 1993 that struck Okushiri Island, Japan, provided high-quality data for tsunami researchers. Since maximum tsunami runup mark was discovered at the tip of a very narrow gulley within a small cove at Monai, a laboratory benchmark was designed based on Monai valley bathymetry and tsunami wave which struck this area. Based on high resolution seafloor bathymetry existed before the event a 1/400 laboratory model of Monai was constructed in a 205m-long, 6m deep, and 3.5m-wide tank at Central Research Institute for Electric Power Industry (CRIEPI) in Abiko, Japan and partly shown in Figure 21. The incident wave from offshore, at the water depth of d = 13.5 cm is known and it is shown in Figure 22. There are reflective vertical sidewalls at y = 0 and 3.5 m (Figure **??**). The entire computational area for the laboratory test is 5.448m $\times 3.402$m, and the grid sizesrecommended for numerical simulations are $\Delta x = \Delta y = 1.4$cm. However, due to numerical limitations, computational domain that is used in numerical simulation is longer in order to generate waves without any reflection disturbance from the back wall(12.488m $\times 3.402$m)(Figure 24). The input wave is a LDN with a leading-depression height of 2.5 mm with a crest of 1.6 cm behind it which is produced in the model using FFT analysis and WK TIME SERIES wavemaker option(Figure 22). Data for water surface elevations during the laboratory experiment is given and compared with numerical simulations at three locations (Gauge 5, 7 and 9), i.e., (x, y) = (4.521, 1.196), (4.521, 1.696), and (4.521, 2.196) in meters (Figure 25). Figure 26 represents the comparison between extracted movie frames from the overhead movie of the laboratory experiment and numerical simulation. Finally, maximum runup in the narrow galley in the numerical solution was 7.43cm which is comparable with the laboratory data (maximum runup of 7.5cm in the lab data or 30m in field tsunami data).

Figure 21: Bathymetric profile for experimental setup for Monai Valley experiment(2007, Figure A24)).

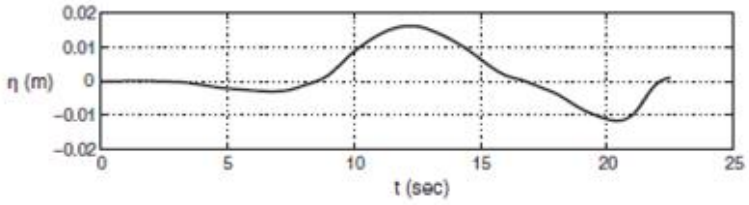

Figure 22: Initial wave profile for Monai Valley experiment (2007, Figure A25)).

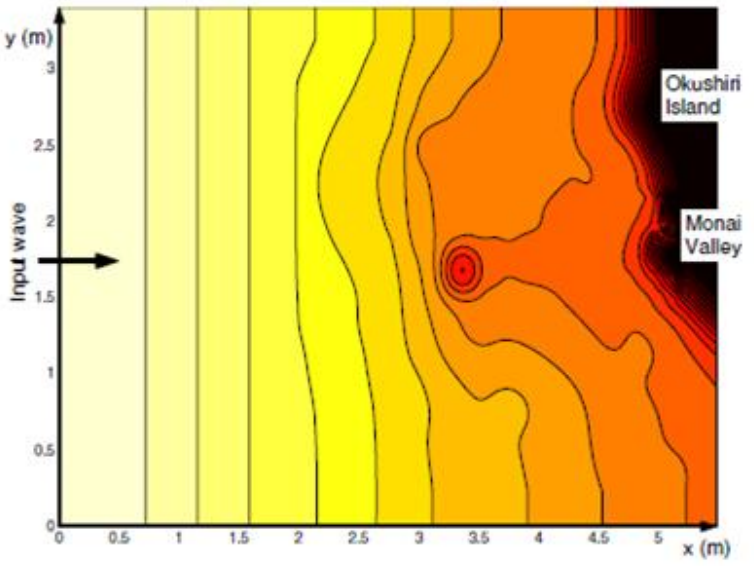

Figure 23: Computational area for Monai Valley experiment(2007, Figure A26)).

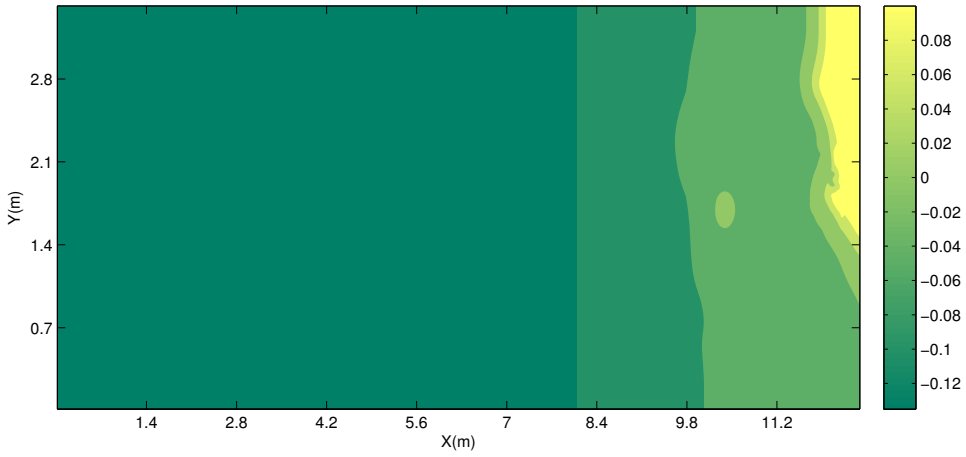

Figure 24: Computational area for Monai Valley numerical simulation.

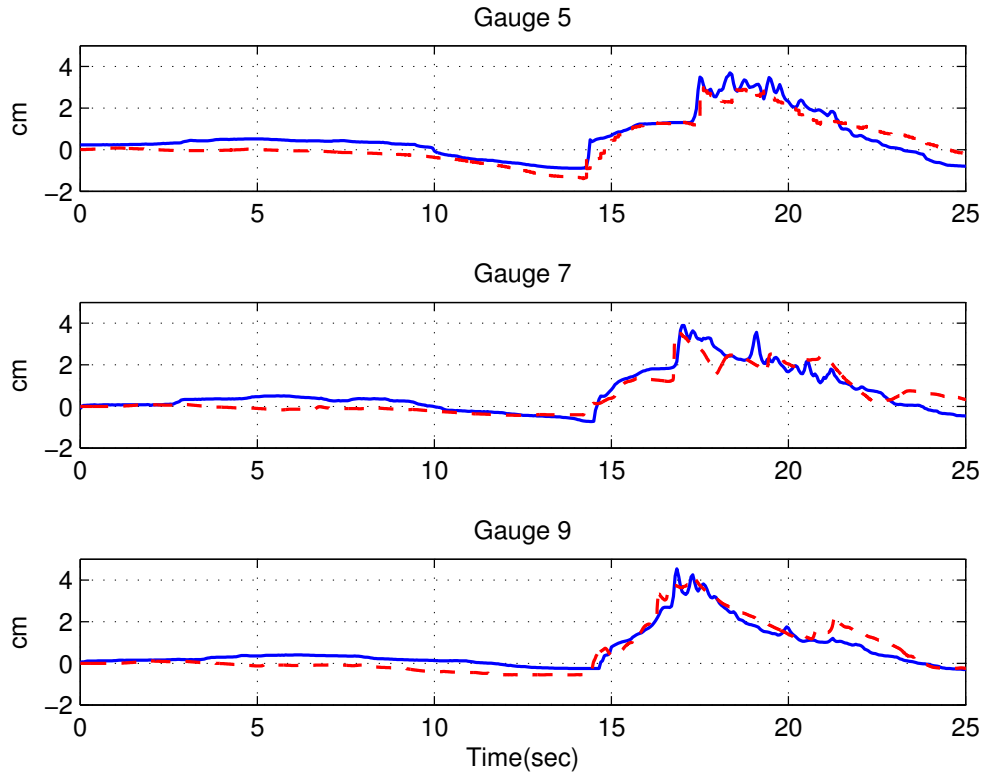

Figure 25: Comparison of computed and measured time series of free surface. Dashed lines: Computed, Solid lines: Measured.

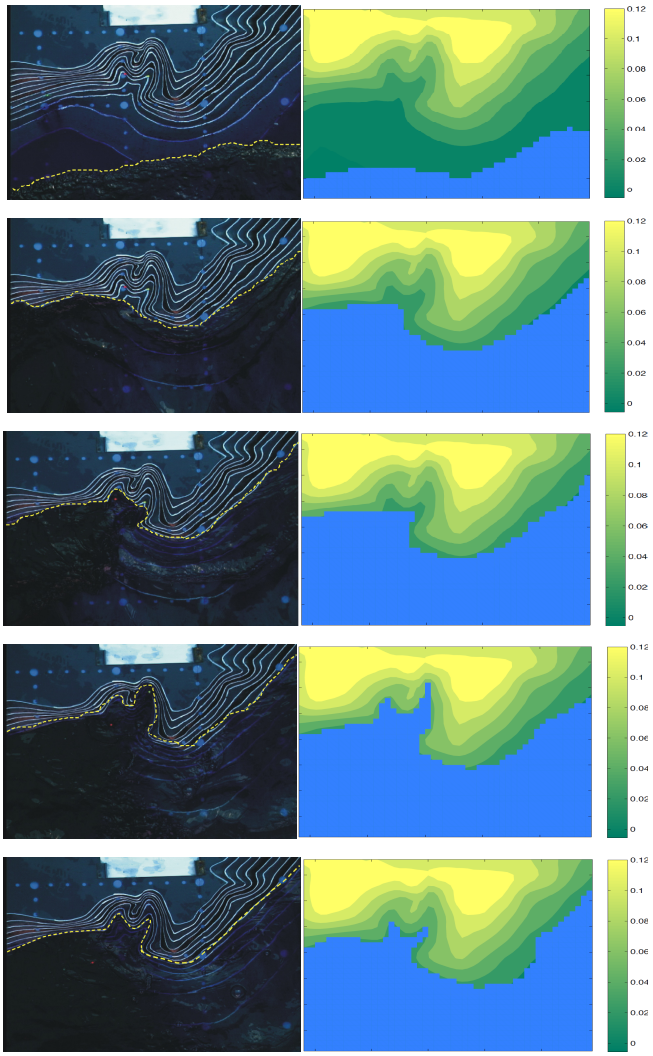

Figure 26: Comparison between extracted movie frames from the overhead movie of the laboratory experiment (left) (from http://burn.giseis.alaska.edu/file_doed/Dmitry/BM7_description.zip) and numerical simulation (right).

References

Briggs, M. J., Synolakis, C. E., Harkins, G. S. and Green, D., 1995, "Laboratory experiments of tsunami runup on a circular island", *Pure Appl. Geophys.*, **144**, 569-593.

Chen, Q., Kirby, J. T., Dalrymple, R. A., Kennedy, A. B. and Chawla, A., 2000, "Boussinesq modelling of wave transformation, breaking and runup. II: Two horizontal dimensions", *J. Waterway, Port, Coast. Ocean Engnrng*, **126**, 48-56.

Chen, Q., Kirby, J. T., Dalrymple, R. A., Shi, F. and Thornton, E. B., 2003, "Boussinesq modelling of longshore currents", *J. Geophys. Res.*, **108**(C11), 3362, doi:10.1029/2002JC001308.

Chen, Q., 2006, "Fully nonlinear Boussinesq-type equations for waves and currents over porous beds", *J. Eng. Mech.*, **132**, 220-230.

Gottlieb, S., Shu C.-W., and Tadmore, E., 2001, "Strong stability-preserving high-order time discretization methods", *SIAM Review*, **43** (1), 89 - 112.

Kennedy, A. B., Kirby, J. T., Chen, Q. and Dalrymple, R. A., 2001, "Boussinesq-type equations with improved nonlinear performance", *Wave Motion*, **33**, 225-243.

Kim, D. H., Cho, Y. S. and Kim, H. J., 2008, "Well balanced scheme between flux and source terms for computation of shallow-water equations over irregular bathymetry", *J. Eng. Mech.*, **134**, 277-290.

Kirby, J. T., Wei, G., Chen, Q., Kennedy, A. B. and Dalrymple, R. A., 1998, " FUNWAVE 1.0, Fully nonlinear Boussinesq wave model. Documentation and user's manual", Research Report No. CACR-98-06, Center for Applied Coastal Research, University of Delaware.

Liang, Q. and Marche, F., 2009, "Numerical resolution of well-balanced shallow water equations with complex source terms", *Adv. Water Res.*, **32**, 873 - 884.

Liu, P. L.-F., Cho, Y. S., Briggs, M. S., Kânoğlu, U. and Synolakis, C. E., 1995, "Runup of solitary waves on a circular island", *J. Fluid Mech.*, **320**, 259-285.

Naik, N. H., Naik, V. K., and Nicoules, M., 1993, "Parallelization of a class of implicit finite difference schemes in computational fluid dynamics", *Int. J.High Speed Computing*, **5**, 1-50.

Nwogu, O., 1993, "An alternative form of the Boussinesq equations for nearshore wave propagation", *J. Waterway, Port, Coastal, and Ocean Engineering*, **119**, 618-638.

O'Sullivan, B., 2009, *Mercurial: The definitive guide*, O'Reilly Media Inc.

Roeber, V., Cheung, K. F., and Kobayashi, M. H., 2010, "Shock-capturing Boussinesq-type model for nearshore wave processes", *Coastal Engineering*, **57**, 407-423.

Rogers, B. D., Borthwick, A. G. L., and Taylor, P. H., 2003, "Mathematical balancing of flux gradient and source terms prior to using Roe's approximate Riemann solver", *J. Comp. Phys.*, **192**, 422-451.

Russel, J.S., 1845, "Report on waves", *Rp. Meet. Brit. Assoc. Adv. Sci. 14th*, 311? 390, John Murray, London.

Shi, F., Dalrymple, R. A., Kirby, J. T., Chen, Q. and Kennedy, A., 2001, "A fully nonlinear Boussinesq model in generalized curvilinear coordinates", *Coastal Engineering*, **42**, 337-358.

Shi, F., Kirby, J. T., Harris, J. C., Geiman, J. D. and Grilli, S. T., 2011a, "A high-order adaptive time-stepping TVD solver for Boussinesq modelling of breaking waves and coastal inundation", In Prepration for Ocean Modelling.

Shi, F., Kirby, J. T., Tehranirad, B., Harris, J. C. and Grilli, S. T., 2011b, "FUNWAVE-TVD Version 1.0. Fully nonlinear Boussinesq wave model with TVD solver. Documentation and user's manual", Research Report No. CACR-11-04, Center for Applied Coastal Research, University of Delaware.

Shiach, J. B. and Mingham, C. G., 2009, "A temporally second-order accurate Godunov-type scheme for solving the extended Boussinesq equations", *Coast. Eng.*, **56**, 32-45.

Synolakis, C.E., 1986, "The runup of long waves", Ph.D. Thesis, California Institute of Technology, Pasadena, California, 91125, 228 pp.

Synolakis, C.E., 1987, "The runup of solitary waves", *J. Fluid Mech.*, **185**, 523?545.

Synolakis, C. E., Bernard, E. N., Titov, V. V., Kânoğlu, U. and González, F. I., 2007, "Standards, criteria, and procedures for NOAA evaluation of tsunami numerical models", NOAA Tech. Memo. OAR PMEL-135, Pacific Marine Env. Lab., Seattle.

Tadepalli, S. and C.E. Synolakis, 1994, "The runup of N-waves on sloping beaches", *Proc. R. Soc. A*, **445**, 99-112.

Tonelli, M. and Petti, M., 2009, "Hybrid finite volume - finite difference scheme for 2DH improved Boussinesq equations", *Coast. Engrng.*, **56**, 609-620.

Wei, G., Kirby, J.T., Grilli, S.T., Subramanya, R., 1995, "A fully nonlinear Boussinesq model for surface waves: Part I. Highly nonlinear unsteady waves", *J. Fluid Mech.*, **294**, 71-92.

Yamamoto, S. and Daiguji, H., 1993, "Higher-order-accurate upwind schemes for solving the compressible Euler and Navier-Stokes equations", *Computers and Fluids*, **22**, 259-270.

Yamamoto, S., Kano, S. and Daiguji, H, 1998, "An efficient CFD approach for simulating unsteady hypersonic shock-shock interference flows", *Computers and Fluids*, **27**, 571-580.

Zhou, J. G., Causon, D. M., Mingham C. G., and Ingram, D. M., 2001, "The surface gradient method for the treatment of source terms in the shallow-water equations", *J. Comp. Phys.*, **168**, 1-25.